Applied Surface Science 386 (2016) 418–426

Contents lists available at ScienceDirect

Applied Surface Science

journal homepage: www.elsevier.com/locate/apsusc

Electrodeposition of flower-like platinum on electrophoretically grown nitrogen-doped graphene as a highly sensitive electrochemical non-enzymatic biosensor for hydrogen peroxide detection

M.T. Tajabadi[a,b], M. Sookhakian[a,b,c,*], E. Zalnezhad[c,**], G.H. Yoon[c], A.M.S. Hamouda[d], Majid Azarang[b], W.J. Basirun[b,e], Y. Alias[a,b,***]

[a] University Malaya Centre for Ionic Liquids, Department of Chemistry, Faculty of Science, University of Malaya, Kuala Lumpur 50603, Malaysia
[b] Department of Chemistry, Faculty of Science, University of Malaya, Kuala Lumpur 50603, Malaysia
[c] Department of Mechanical Convergence Engineering, Hanyang University, 222 Wangsimni-ro, Seongdong-gu, Seoul, 133-791, Korea, Korea
[d] Mechanical and Industrial Engineering Department, College of Engineering, Qatar University, 2713, Doha, Qatar
[e] Institute of Nanotechnology & Catalysis Research, Institute of Postgraduate Studies, University Malaya, 50603 Kuala Lumpur, Malaysia

ARTICLE INFO

Article history:
Received 15 March 2016
Received in revised form 30 May 2016
Accepted 9 June 2016
Available online 14 June 2016

Keyword:
Nitrogen doped graphene
Electrophoretic deposition
Platinum
Electrodeposition
Hydrogen peroxide
Biosensor

ABSTRACT

An efficient non-enzymatic biosensor electrode consisting of nitrogen-doped graphene (N-graphene) and platinum nanoflower (Pt NF) with different N-graphene loadings were fabricated on indium tin oxide (ITO) glass using a simple layer-by-layer electrophoretic and electrochemical sequential deposition approach. N-graphene was synthesized by annealing graphene oxide with urea at 900 °C. The structure and morphology of the as-fabricated non-enzymatic biosensor electrodes were determined using X-ray diffraction, field emission electron microscopy, transmission electron microscopy, Raman and X-ray photoelectron spectra. The as-fabricated Pt NF-N-graphene-modified ITO electrodes with different N-graphene loadings were utilized as a non-enzymatic biosensor electrode for the detection of hydrogen peroxide (H_2O_2). The behaviors of the hybrid electrodes towards H_2O_2 reduction were assessed using chronoamperometry, cyclic voltammetry and electrochemical impedance spectroscopy analysis. The Pt NF-N-graphene-modified ITO electrode with a 0.05 mg ml^{-1} N-graphene loading exhibited the lowest detection limit, fastest amperometric sensing, a wide linear response range, excellent stability and reproducibility for the non-enzymatic H_2O_2 detection, due to the synergistic effect between the electrocatalytic activity of the Pt NF and the high conductivity and large surface area of N-graphene.

1. Introduction

Nanoelectroanalytical chemistry is an expanding multidisciplinary field, which combines the unique properties of nanomaterials (e.g., optical, magnetic, electronic, mechanical and catalytic properties) with the electrochemical characterizations (e.g., low cost, rapid detection and high sensitivity) for the fabrication of various application devices, such as fuel cells, supercapacitors, catalyst and sensor devices [1]. Among these applications, electrochemical biosensors, especially non-enzymatic biosensors, have received tremendous attention due to several advantages such as low cost, simplicity, high selectivity and sensitivity. Although non-enzymatic biosensors can avoid the intrinsic defects of enzymatic biosensors, especially environmental factors, such as temperature, oxygen, pH and coexisting chemicals; the kinetics and overpotential of the electrochemical reaction are crucial factors that influence the Faradaic current and analytical performance [2]. Therefore, these sensors could be affected by electrode modification.

Currently, many efforts have been focused on electrode modification for the preparation of new electrocatalytic materials to improve the kinetics of electron transfer. Therefore, noble metal catalysts, such as Au, Ag, Pd and especially Pt, have received wide recognition in non-enzymatic biosensors. In addition, Pt exhibits high catalytic activity for numerous reactions and has found appli-

* Corresponding author at: University Malaya Centre for Ionic Liquids, Department of Chemistry, Faculty of Science, University of Malaya, Kuala Lumpur 50603, Malaysia.
** Corresponding author.
*** Corresponding author at: University Malaya Centre for Ionic Liquids, Department of Chemistry, Faculty of Science, University of Malaya, Kuala Lumpur 50603, Malaysia.
E-mail addresses: m.sokhakian@gmail.com, m.sokhakian@siswa.um.edu.my (M. Sookhakian), erfan@hanyang.ac.kr (E. Zalnezhad), yatimah70@um.edu.my (Y. Alias).

http://dx.doi.org/10.1016/j.apsusc.2016.06.045
0169-4332/

cation in various fields, such as catalytic hydrogenation, oxygen reduction and fuel-cell catalysis [3]. However, Pt is expensive and rare, and new strategies are needed to limit the amount of Pt required for various technological applications. Therefore, the support materials on which the Pt catalysts are attached, have also received much attention because they play a crucial role in enhancing the analytical performance. The support materials of the catalysts are influenced by many factors such as the hydrophobicity, biocompatibility, the surface roughness and morphology. Therefore, an ideal catalyst support material as the sensing interface should possess a strong affinity towards the catalyst particles for their immobilization, high electrical conductivity and good chemical stability. In addition, this material should be non-toxic and possess a high surface area and long-term stability [4]. Therefore, materials such as redox proteins [5], conductive polymers [6] and carbon [7], have been utilized as support materials for non-enzymatic biosensors.

Graphene nanosheet, a layer of two-dimensional sp^2-hybridized carbon atoms, has gathered huge interest as an alternative and effective support material because of the high surface area (2630 m^2/g), high conductivity (10^3–10^4 s/m), high electrical mobility (200000 $cm^2\,V^{-1}\,s^{-1}$), and high chemical stability [8–10]. These amazing physical and chemical characteristics offer bright prospects in electronics [11], photonics [12], supercapacitors [13], catalysis [14], batteries [15] and dye-sensitized solar cells applications [16]. However, the aggregation of graphene during the fabrication of the electrocatalyst nanostructures, could dramatically decrease the surface area [17] and thereby lead to a significant decrease in the conductivity [17]. Therefore, the functionalization or doping of the graphene lattice with atoms such as boron, nitrogen, phosphorous and sulfur, is an effective strategy to modulate the surface chemistry and the electronic properties of graphene [18]. Among these heteroatoms, nitrogen is best dopant because of the similar atomic radius and valence electrons for the bonding with carbon atoms. Furthermore, the graphene π-electronic system and the lone pair of the nitrogen atoms can form strong valence bonds. This will lead to a significant improvement of the electronic properties of graphene, which promotes to a uniform dispersion and fast nucleation growth kinetics of the catalyst nanostructures. In addition, the nitrogen doping increases the conductivity of graphene with the increase of the Fermi level closer to the conduction band [19], which improves the sensitivity of non-enzymatic biosensors. In the past, different methods have been utilized to produce nitrogen-doped graphene (N-graphene), such as chemical vapor deposition (CVD)[20], thermal annealing [21] and direct-current arc discharge, with different nitrogen precursors [22]. However, a detail investigation of the N-graphene loading and its influence on the analytical performance of non-enzymatic biosensors is needed to produce platinum nanoflower (PT NF)-loaded N-graphene catalyst materials.

Herein, for the first time, we reported a layer-by-layer electrochemical deposition route for the rapid synthesis of Pt NF ensemble as a second layer on N-graphene-modified indium tin oxide (ITO) electrodes. As the primary layer, N-graphene was synthesized via the annealing graphene oxide (GO) with urea at 900 °C, followed by electrophoretic deposition on ITO electrodes. The electrochemical and electrophoretic depositions are simple controllable processes and environmentally benign, and produce uniform deposits with high purity. The nanoflower morphology of Pt possesses a porous structure, with large surface areas and active centers for enhanced analytical performance. The as-fabricated Pt NF-N-graphene-modified ITO electrodes with different N-graphene loadings were utilized as non-enzymatic H_2O_2 sensors, to gain a better understanding on the effects of N-graphene loading on the analytical performance of H_2O_2 detection. The Pt NF-N-graphene-modified ITO with 0.05 mg ml^{-1} N-graphene loading exhibited improved properties for H_2O_2 detection over a linear range between 1 μM to 1 mM.

2. Experimental methods

2.1. Chemicals

Analytical grade chemicals (i.e., NaH_2PO_4, Na_2HPO_4, 30 wt% H_2O_2 and H_2PtCl_6) were procured from Sigma Aldrich and dissolved in double-distilled water (resistance = 18.3 MΩ). Stock solutions of NaH_2PO_4 and Na_2HPO_4 were used to prepare the phosphate-buffered (PBS) solution. The experimental detection was performed with a fresh H_2O_2 solution.

2.2. Synthesis of N-graphene

Graphite powder (1–2 μm, Aldrich) was utilized for the synthesis of graphene oxide (GO) according to the modified Hummers method [23]. The synthesis of N-graphene is described elsewhere [24]. Briefly, 50 ml of a GO dispersion in ethanol (1 mg/mL) was added with 100 mg of urea. The dispersion was heated to 80 °C with stirring until it dried. The powders were then placed in an Al_2O_3 crucible in a tube furnace and flushed with Ar gas to completely remove the oxygen in the medium. After the flow of Ar gas (100 sccm), the temperature was increased to 600 °C at a heating rate of 3 °C min^{-1} for one hour. Then, the temperature was increased to 900 °C at a rate of 5 °C min^{-1}. The process was maintained at 900 °C for 4 h, then the furnace was cooled to room temperature, to collect the as-synthesized N-graphene.

2.3. Electrophoretic deposition (EPD) of N-graphene-modified ITO

The set-up for the EPD was published previously [18]. The suspension contained 40 ml of different concentrations of N-graphene (0.01 mg ml^{-1}, 0.05 mg ml^{-1}, and 0.1 mg ml^{-1}) in 0.025 M $Mg(NO_3)_2$ in isopropyl alcohol, and was sonicated for 30 min to obtain a homogeneous suspension. Before the ITO glass substrates (10 mm × 20 mm) were washed in acetone and distilled water, they were immersed for a few minutes in a 5% HF solution to remove the oxide layer. The two ITO electrodes were immersed vertically in the suspension with a distance of 10 mm from each other. The DC potential and deposition time were 20 V and 5 min, respectively. Finally, the freshly coated electrodes were dried at 50 °C in an oven.

2.4. Electrochemical deposition of Pt NF

The fresh N-graphene-modified ITO thin film electrodes with different N-graphene loadings were utilized as the working electrode (WE) for the Pt NF deposition by cyclic voltammetry, in five voltammetric cycles. An Ag/AgCl and a platinum wire were the reference (RE) and counter electrodes (CE), respectively. The solution contained 20 μl of H_2PtCl_6 in 15 ml of a 0.05 M $Mg(NO_3)_2$ as the supporting electrolyte. The potential scan was from −0.2 to −0.8 V at 10 mV s^{-1}. The as-fabricated Pt NF-N-graphene-modified ITO thin film electrodes with different N-graphene loadings (i.e., 0.01 mg ml^{-1}, 0.05 mg ml^{-1}, and 0.1 mg ml^{-1}) are referred as PNG-1, PNG-2 and PNG-3, respectively. The electrochemical deposition of pure Pt NF-modified-ITO was performed with the same procedures. The electrodes were washed with distilled water and finally dried at 50 °C in an oven.

2.5. Characterization

A X-ray powder diffractometer (XRD, PANalytical's Empyrean) with a monochromated CuKa radiation (l = 1.54056 Å) was used to characterize the powders. A transmission electron microscope

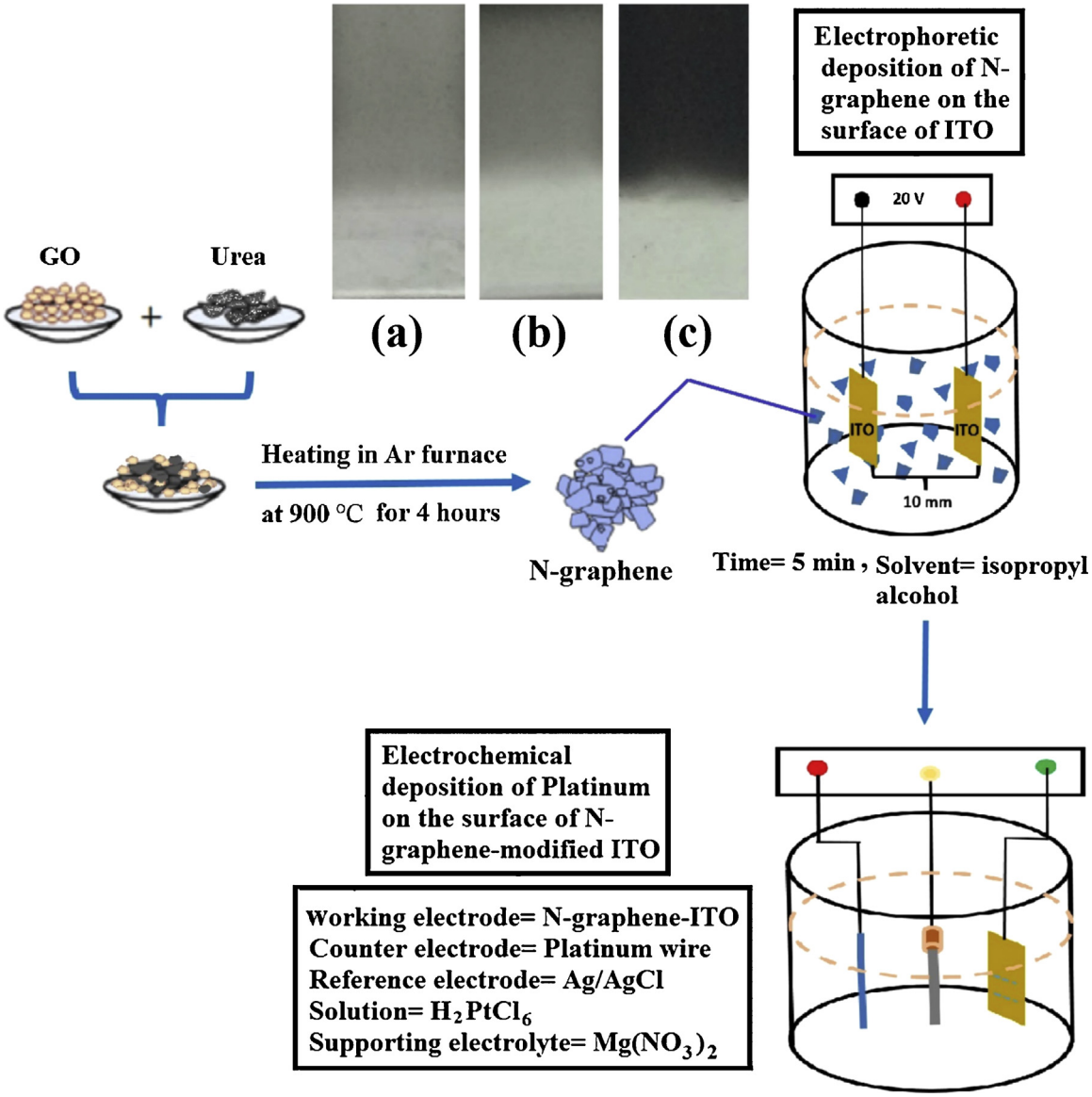

Fig. 1. The schematic of the overall fabrication of PNG-modified-ITO electrode and photographic images of N-graphene-modified ITO with different concentrations of N-graphene: (a) 0.01 mg ml^{-1}, (b) 0.05 mg ml^{-1}, and (c) 0.1 mg ml^{-1}.

(500 kV, TEM-FEIG-4020) and field emission scanning electron microscope (FESEM-Hitachi SU8000) were utilized to examine the particle sizes and the morphology of the electrodes. The electrodes were ultrasonicated in distilled water prior to the characterization. The spectroscopic measurements were performed using an ESCALAB MK II X-ray photoelectron spectrometer (Mg excitation source) for the X-ray photoelectron spectroscopy (XPS) analysis while a Renishaw Invia Raman Microscope instrument (laser excitation, l = 514 nm) was utilized for the Raman spectroscopy analysis. The electrochemical experiments were performed using a potentiostat/galvanostat (Autolab PGSTAT30, Ecochemie Netherlands).

3. Results and discussions

3.1. Characterization of Pt-NG-modified ITO electrode

Fig. 1 shows the schematic illustration of the overall synthesis procedure for Pt-NG-modified ITO electrode and N-graphene on ITO electrodes prepared by the electrophoretic deposition. As the N-graphene loading increased, the thin film electrodes were grayish in color due to the increasing thickness of the N-graphene film (Fig. 1(a–c)). The first cycle in the cyclic voltammograms (CVs) of the electrodeposited Pt NF on the surface of N-graphene-modified ITO with 0.05 mg ml^{-1} N-graphene loading is shown in Fig. 2. Two reduction peaks and one oxidation peak were observed in the negative scan, which indicates the successful reduction of the Pt NF. According to Zangari et al. [25], the electrochemical deposition of Pt from the H_2PtCl_6 electrolyte involves a-three step mechanism:

$$PtCl_6^{2-} + 2e^- \rightarrow PtCl_4^{2-} + 2Cl^- \quad (1)$$

$$PtCl_4^{2-} + 2e^- \rightarrow Pt + 4Cl^- \quad (2)$$

and/or

$$PtCl_6^{2-} + 4e^- \rightarrow Pt + 6Cl^- \quad (3)$$

The peak at −0.38 V might be due to the reduction of Pt (IV) to Pt (II) (Eq. (1)) or Pt (IV) to Pt (0) (Eq. (3)). The small wave which begins at approximately −0.65 V, could be due to the electrochemical reduction of Pt (II) to Pt (0) (Eq. (2)). However, the anodic

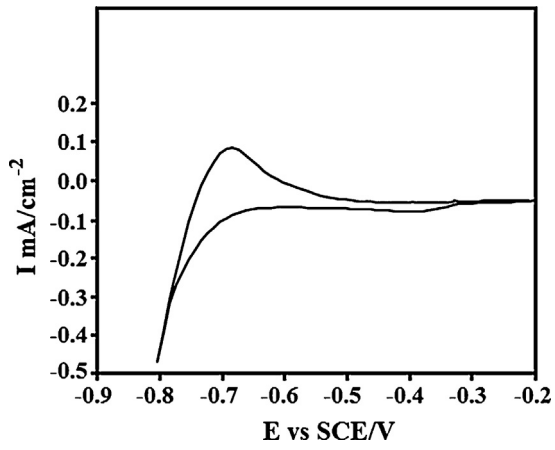

Fig. 2. CV of the as-electrodeposited Pt NF-N-graphene (0.05 mg ml^{-1})-modified ITO electrode.

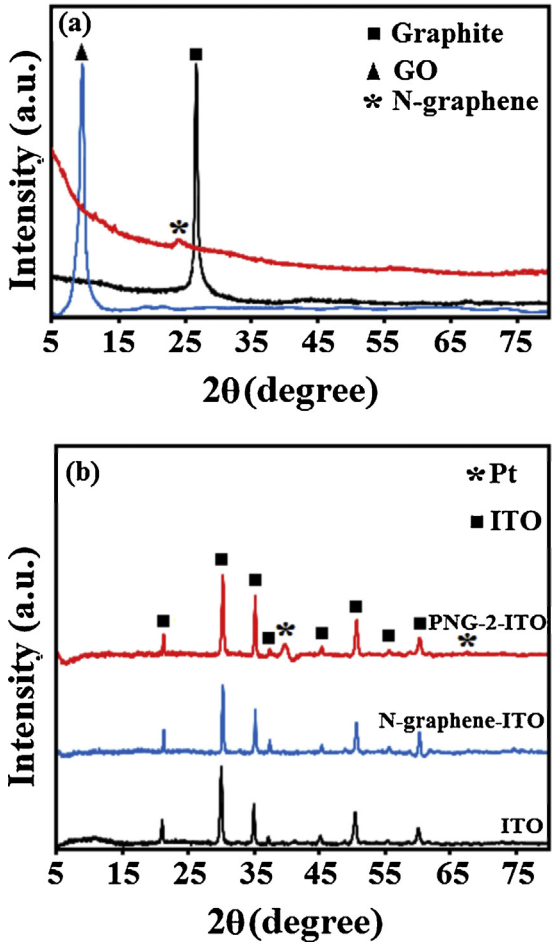

Fig. 3. (a) XRD of graphite, GO and N-graphene. (b) XRD of the bare ITO, N-graphene-ITO and PNG-2 electrodes.

peak on the reverse scan is most likely due to the desorption and electrooxidation of the strongly adsorbed hydrogen [25].

Fig. 3(a) shows the XRDs of graphite, GO and N-graphene. The XRD for GO shows a sharp diffraction peak at 2θ = 10.6°, is due to the (001) lattice plane, with a d-spacing of 0.83 nm. This d-spacing is much wider than the narrow peak at 26.8° (graphite), with an interlayer spacing of 0.33 nm. This result suggests that the raw graphite was exfoliated into GO sheets, from the presence of the oxygen, carboxyl and other functional groups [17]. For comparison, after the annealing of GO with urea at 900 °C in Ar for 4 h, the diffractogram shows the absence of this strong peak, along with the presence of a broad (002) diffraction peak centered at 2θ of 24.86°, which corresponds to an interlayer spacing of 0.35 nm. This result indicates the formation of graphene, from the removal of the oxygen functional groups during the annealing process [26]. The crystalline structure of the Pt NF-modified ITO electrode and PNG-2 are shown in Fig. 3(b). The N-graphene-modified ITO electrode exhibits XRD patterns that are similar to those of the blank ITO electrode, which, is due to the small amount of N-graphene. Compared to the N-graphene-modified ITO, the spectra of the PNG-2-modified ITO electrode (after electrodeposition of Pt NF in 5 cycles) contain diffraction peaks at 2&z.Theta; values of 39.765° and 67.456°, which is indexed to the (111) and (220) lattice planes, respectively, of cubic platinum (JCPDS card no. 00-004-0802) with the following lattice constants: a = b = c = 3.923 Å.

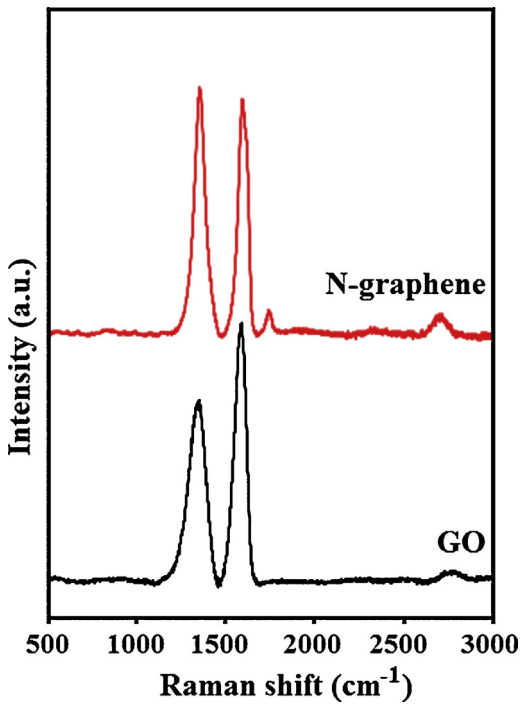

Fig. 4. Raman spectra of GO and N-graphene.

Raman spectroscopy was also utilized to further investigate the structural and electronic properties of the as-synthesized N-graphene. Fig. 4 compares the Raman spectra of pristine GO and N-graphene after the annealing with urea at 900 °C. The Raman spectra of GO contain three peaks located at 1359, 1588 and 2688 cm^{-1}, corresponding to the D, G and 2D bands, respectively. The G band is the result of the in-plane bond stretch of the C—C sp^2 bond, and the D band is attributed to the different types of defects, such as the vacancy-like and sp^3 defects. These defects are the product of hydrogenation, oxidation, electron doping, domain boundaries and grain boundary edges[18]. In addition to these three peaks, N-graphene exhibits an extra weak *D′* band located at 1710 cm^{-1} [27]. However, the major difference between N-graphene and GO is the degree of disorder, which can be observed from the intensity ratio of the D and G bands (I_D/I_G). The intensity ratio (I_D/I_G) of GO and N-graphene are 0.66 and 1.28, respectively. The increase of the (I_D/I_G) ratio implies that the annealing process created a large amount of sp^2 bonds and structural defects in the N-graphene lattice. The intensity of the 2D band which is attributed to a two-phonon double-resonant process, is reciprocal to the rate of the electron-hole scattering process [18]. Therefore, the increased intensity of the 2D peak at 2703 cm^{-1} is from the increase of the

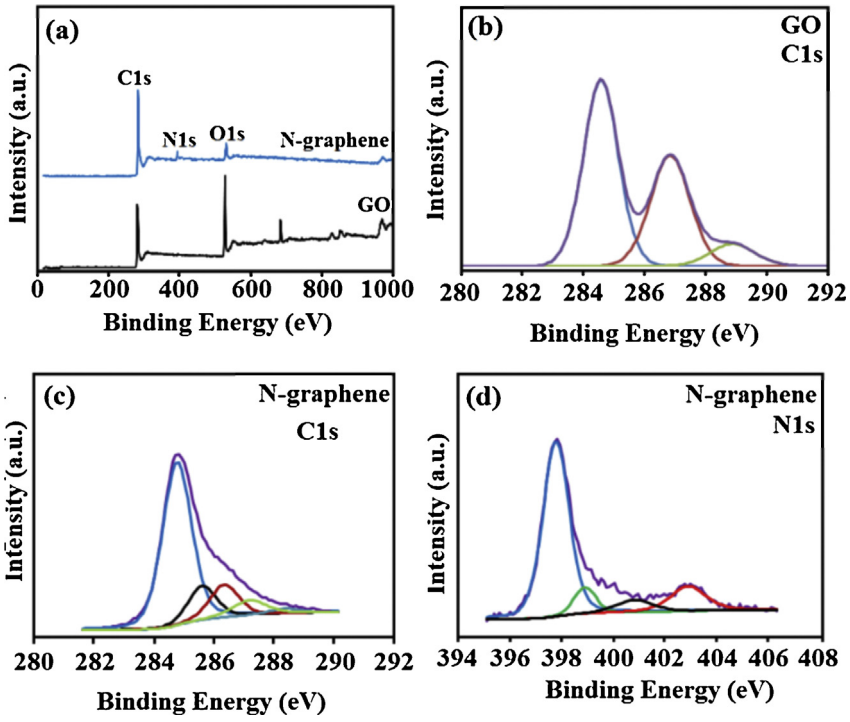

Fig. 5. (a) Wide scan XPS spectra of GO and N-graphene. The high-resolution XPS spectra of (b) C1s of GO (c) C1s of N-graphene, and (d) N1 s of N-graphene.

N-graphene layers compared to what is observed in GO, after the annealing with urea [17].

Fig. 5 shows the X-ray photoelectron spectra (XPS) of GO and the nitrogen-bonded groups in N-graphene. The wide-scan XPS spectrum of GO shows the presence of oxygen and carbon. The wide-scan XPS spectrum of N-graphene shows the presence of nitrogen doping in graphene during the annealing of GO with urea (Fig. 5(a)). The GO spectrum shows a C1 s peak at 283.2 eV and a O1 s peak at 531.6 eV [18]. The C:O atomic ratio is 0.69 but the O1 s peak intensity decreased significantly. The C:O atomic ratio of 2.36 indicates the successful reduction of GO, after the annealing with urea. Moreover, the N-graphene spectrum shows the N1 s peak at 398.6 eV with a N:C atomic ratio of 0.56 (Fig. 5(a)). The oxygen functional groups of GO and N-graphene were identified by the deconvolution of the C1 s peak. The high-resolution C1 s spectrum of GO in Fig. 5(b) was deconvoluted into two peaks at 286.9 and 284.6 eV, attributed to the C—O hydroxyl and C—C epoxide groups, respectively. The smaller peak at 288.8 eV was attributed to the O—C=O of GO [18]. The C1 s spectrum of N-graphene and GO have the same type of oxygen atoms but the N-graphene spectrum shows a decrease in the C—O and O—C=O intensities after the annealing with urea. This result confirms the recovery of the π-electron network of graphene after the annealing process, as shown in Fig. 5(c) [18]. Moreover, the C—N groups at 285.7 eV suggest that the nitrogen atoms were incorporated into the graphene nanosheets during the annealing process with urea. A detailed information about the nitrogen functional groups can be provided by the deconvolution of the N1 s peak in the N-graphene XPS spectrum. As shown in Fig. 5(d), the N1 s peak was deconvoluted into four different regions at 397.9, 399.8, 400.8 and 402.9 eV, which were attributed to the four different types of N-containing groups (i.e., pyridinic N—C, pyrrolic N—C, quaternary N—C and oxidized-N of pyridine, respectively) [28]. In the pyridinic N—C structure, the N atoms are situated at the edge of the graphene plane, each N atom donates one π-electron to the graphene π-electron system and is bonded to two C atoms. While in the pyrrolic N—C, each N atom contributes two π-electrons to the graphene π-electron network and is bonded to two C atoms. The nitrogen atoms in the quaternary-N—C structures are bonded to three carbon atoms. In addition, the oxidized nitrogens are mostly the nitrogen atoms in the pyridine group, are bonded to one oxygen atom and two carbon atoms.

FESEM analysis was performed to study the morphology of the Pt NF-N-graphene hybrid (Fig. 6). The low magnification FESEM image of the as-electrodeposited Pt NF on the surface of the N-graphene-modified ITO (Fig. 6(a)) shows the presence of Pt forms nanoflower-like structures. In addition, the Pt NF was uniform and densely distributed on the surface of the electrophoretically deposited N-graphene-modified ITO electrode. A careful and closer view (Fig. 6(b)) reveals that the individual Pt NFs are quasi-spherical in appearance with sizes in range of 250–300 nm.

A more detalied investigation of the morphology of the N-graphene and Pt NFs was performed using the TEM technique. The TEM image reveals that the Pt nanoflowers are highly decorated on the surface of N-graphene. In addition, the N-graphene exhibits a crumpled sheet-like layer morphology that were several micrometers in diameter (Fig. 7(a)). The crumpling effect may be due to the defective structures formed during the exfoliation or the doping of nitrogen atoms. The high magnification TEM image of the Pt NF (Fig. 7(b)) shows that each Pt NF consists of randomly shaped nanofibers that point radially outward, and the nanofibers were assembled from tens to hundreds of self-assembled particles growing in all directions.

3.2. Electrocatalytic activity for H_2O_2 reduction

The detection of H_2O_2 was performed using the Pt NF-N-graphene-modified ITO electrode to gain insight into the effect of N-graphene loading on the analytical performance of the non-enzymatic sensor electrode. The cyclic voltammograms (CVs) of ITO, pure Pt NF-modified ITO, PNG-x (x = 1, 2,and 3)-modified ITO electrode in nitrogen saturated 0.1 M PBS at pH 7.2 with the presence of 0.1 mM H_2O_2 at 50 mV s^{-1} are shown in Fig. 8(a). In Fig. 8(a), the ITO electrode shows the weakest response toward H_2O_2 detection (Inset of Fig. 8a). The pure Pt NF-modified ITO shows a high

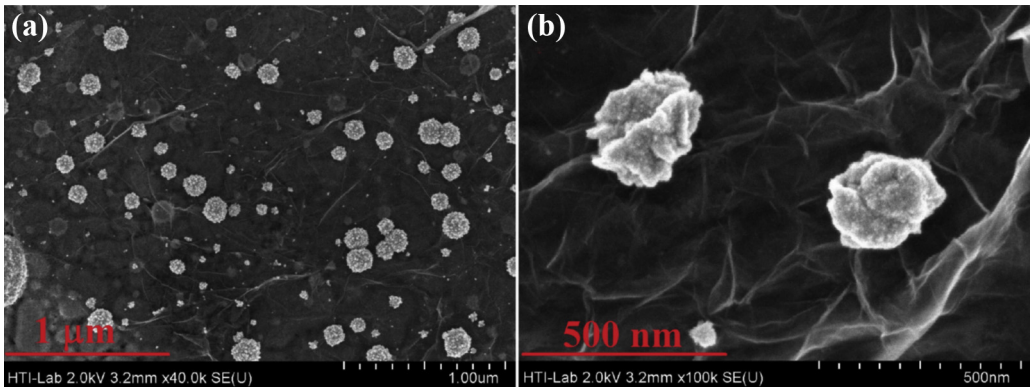

Fig. 6. (a,b) Low and high magnification FESEM images of PNG-2-modified ITO electrodes.

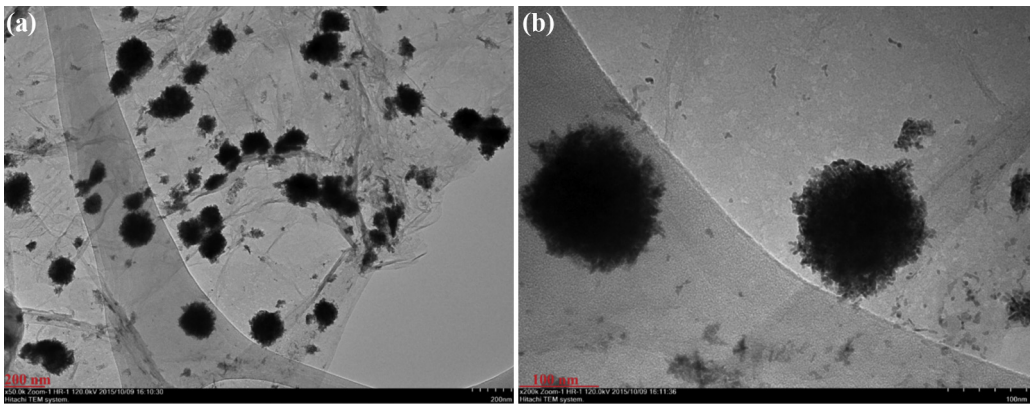

Fig. 7. (a,b) Low and high magnification TEM images of PNG-2.

peak current density of $-0.47\ mA\ cm^{-2}$ at $-0.25\ V$ in the presence of H_2O_2, much higher than the ITO electrode. The presence of N-graphene leads to a remarkable enhancement in the current density response of the pure Pt NF from $-0.47\ mA\ cm^{-2}$ to $-1.12\ mA\ cm^{-2}$ for PNG-1. With an increase in the N-graphene loading up to $0.05\ mg\ ml^{-1}$, the current density increases from $-1.12\ mA\ cm^{-2}$ to $-1.24\ mA\ cm^{-2}$ for both PNG-1 and PNG-2. However, a further increase of the N-graphene concentration to $0.1\ mg\ ml^{-1}$ led to a decrease in the current density from $-1.24\ mA\ cm^{-2}$ to $-0.92\ mA\ cm^{-2}$. The PNG-2 (Pt NF–N-graphene, $0.05\ mg\ ml^{-1}$) gave the strongest response at $-0.40\ V$ with the highest peak current density (2.5-fold higher than the pure Pt NF electrode) for the H_2O_2 reduction. This result demonstrates that the presence of N-graphene enhances the electrocatalytic activity of pure Pt NFs toward H_2O_2 reduction.

The catalytic activity for H_2O_2 reduction was examined by cyclic voltammetry of the PNG-2-modified ITO at various scan rates. Fig. 8(b) shows the CVs of the PNG-2-modified ITO in nitrogen saturated 0.1 M PBS solution at pH 7.2 with 0.1 mM H_2O_2 at various scan rates. The peak currents rise linearly with the scan rate from 10 to $90\ mV\ s^{-1}$. The reduction peak is slightly shifted towards negative region, which may be due to the changes in the activity of the PNG-2-modified ITO during the H_2O_2 reduction. These results indicate that the reduction of H_2O_2 is a surface-controlled process [18].

Fig. 9 shows the effect of the potential on the current density of the PNG-2-modified ITO in nitrogen saturated 0.1 M PBS solution at pH 7.2 in 0.1 mM H_2O_2, between -0.2 to $-0.6\ V$. The plot of current density vs. potential indicates that the current density gradually increases with the potential from -0.2 to $-0.4\ V$. However, a further increase in the potential led to a significant decrease in the current density. The best working potential is selected from the least negative potential, which exhibits a high selectivity and high analyte-dependent current. Therefore, a potential of $-0.40\ V$ was identified as the best working potential for the reduction of H_2O_2.

In addition, the amperometric current-time technique is an effective approach to examine the performance of the fabricated electrochemical sensor. Therefore, the amperometric response of the PNG-2-modified ITO electrode in nitrogen saturated 0.1 M PBS solution with successive additions of H_2O_2 at $-0.40\ V$ vs Ag/AgCl are shown in Fig. 10. The current responses of the PNG-2 hybrid are rapid, steady, prompt (achieving the steady state current within 5 s), and reproducible when H_2O_2 was added to the PBS solution. The corresponding current-concentration and calibration curve was performed three times, and the standard deviations were calculated (the inset of Fig. 10). The current response of the as-fabricated PNG-2 electrode is linear when the H_2O_2 concentration is increased from 1 μM to 1 mM. The linear regression equation is written as $I\ (mA) = 61.23\ (\mu A mM^{-1}\ cm^{-2}) + 2.193$ with a correlation coefficient of 0.9991. The limit of detection (LOD) of the PNG-2-modified ITO electrode was calculated using the following equation [29]:

$$LOD = \frac{3S_B}{b} \quad (4)$$

where b is the slope of the analytical curve and S_B is the standard deviation of the blank solution. The estimated LOD at a signal-to-noise ratio of 3 is 0.34 μM. Moreover, the amperometric response to 0.1 mM H_2O_2 in PBS (0.1 M, pH 7.2) was obtained over a 48 min time period. The PNG-2-modified ITO electrode remained stable throughout the experiment with only 5.1%, 9.8% and 12.4% decreases in the current at 10, 30 and 48 min, respectively. The reproducibility of the modified electrode was evaluated by measur-

Table 1
A summary and comparison of the current results with those from previous studies on the performance of H_2O_2 assays.

Type of electrode	Limit of detection (μM)	Sensitivity (μAmM^{-1})	Linear range (mM)	References
Pt-Carbon nanofiber/GCE	1.7	–	0.005–100	[31]
Pt-Polyaniline/MSF	0.24	50	0.001–2	[32]
Pt-Polypyrrole/GCE	1.2	80.4	1–8	[33]
Pt-Poly melamin/GCE	0.65	–	0.005–1.65	[34]
Pt-PVA-CNT/GCE	0.7	122.63	0.002–3.8	[35]
Pt/Au	60	22.18	0.1–0.9	[36]
N-graphene/GCE	0.05	–	0.005–1.2	[37]
Pt-N-graphene/ITO	0.34	61.23	0.001–1	This work

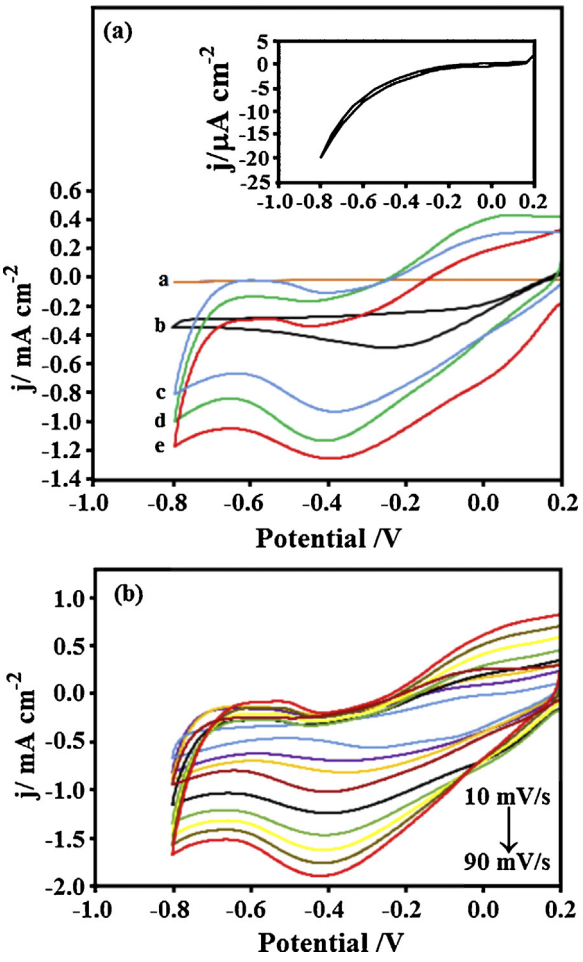

Fig. 8. (a) CVs of ITO (a), Pt NF-modified ITO (b), and PNG-1 (c), PNG-2 (d) and PNG-3 (e), enlarge inset is CVs of ITO. (b) CVs of PNG-2-modified ITO at various scan rates in nitrogen saturated PBS (0.1 M, pH 7.2) with 0.1 mM H_2O_2.

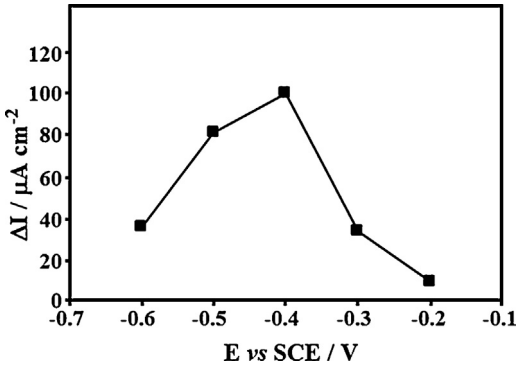

Fig. 9. The current density vs. potential of the PNG-2-modified ITO electrode in 0.1 mM H_2O_2 in 0.1 M PBS at pH 7.2.

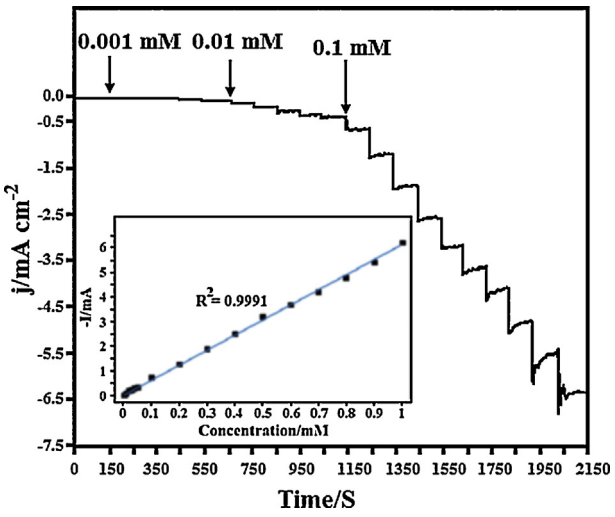

Fig. 10. Typical amperometric response of the PNG-2-modified ITO electrode in nitrogen saturated PBS (0.1 M, pH 7.2). Inset: calibration plot.

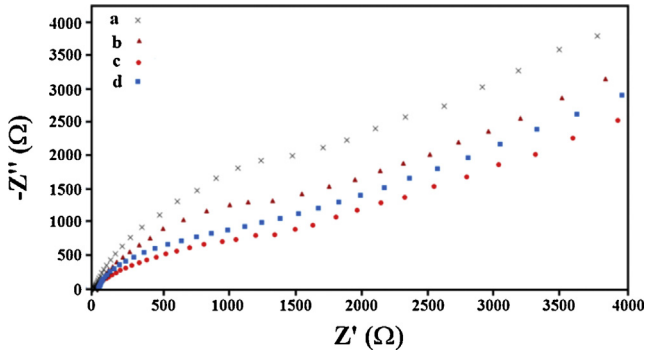

Fig. 11. Nyquist plots of (a) Pt NF, (b) PNG-1, (c) PNG-2, and (d) PNG-3 in 0.1 M KCl solution containing 1 mM $Fe(CN)_6^{3-/4-}$ (1:1).

ing the current response to H_2O_2 under the same conditions. The relative standard deviation (RSD) of the current response to 0.1 mM H_2O_2 was 5.1% for 6 successive determinations. Therefore, the PNG-2-modified ITO electrode exhibits good stability and reproducibility for the electrocatalytic reduction of H_2O_2, and the electrochemical performance of this sensor is comparable to that of the sensors based on other materials, as shown in Table 1.

Based on the CV curves and amperometric responses, N-graphene has an important role in the catalytic enhancement of the Pt NF-modified ITO electrode. Therefore, electrochemical impedance spectroscopy (EIS) technique was performed with a 5 mV AC signal with a frequency range of $0.1–10^5$ Hz to evaluate the charge transfer kinetics and ion diffusion process of the sensor electrodes. Fig. 11shows the Nyquist plots of the pure Pt NF-modified ITO and PNG-x (x = 1, 2, 3)-modified ITO electrodes in 0.1 M KCl solution containing1 mM $Fe(CN)_6^{3-/4-}$ (1:1). The Nyquist

plots of the electrodes exhibit a high-frequency response due to the presence of the charge-transfer resistance (R_{ct}), which is related to the catalytic activity of the reduction of $Fe(CN)_6^{3-}$ to $Fe(CN)_6^{4-}$ across the electrode-electrolyte interface. In addition, the low-frequency response is due to the Warburg diffusion process. The Warburg impedance is attributed to the diffusion controlled process across the deposited layer [29]. As shown in Fig. 11, compared with the pure Pt NF-modified ITO electrode, the presence of N-graphene led to a significant decrease in the diameter of the semicircle at higher frequency, which confirms that the conductivity of the electrode is increased due to the presence of N-graphene in the hybrid electrodes. The increased conductivity apparently enhances the catalytic ability of the sensor electrode for faster electron transfer process across the interface, resulting in an improved catalytic performance of the sensor electrodes. However, the diameter of the semicircle is increased when the N-graphene loading is increased beyond the optimum value (0.05 mg ml^{-1}), which indicates a decrease in the catalytic activity of the PNG-3-modified ITO electrode. This phenomenon can be assigned to the decreased in conductivity of the PNG-3 hybrid electrode compared to the PNG-2 hybrid electrode due to the excessive N-graphene content, leading to larger agglomeration during the electrophoretic deposition, which substantially decreases the surface area [30] and led to a significant decrease in the analytical performance of the sensor electrode.

4. Conclusion

N-graphene nanosheets were successfully grown with different degrees of loading on ITO substrate using EPD. The Raman and XPS results show the reduction and nitrogen doping of graphene oxide to N-graphene during annealing with urea at 900 °C. The Pt NFs were electrodeposited on N-graphene-modified ITO electrode. The Pt NF-N-graphene-modified ITO electrodes with different N-graphene loadings were used as an advanced biosensor electrode for H_2O_2 detection. The presence of N-graphene in the Pt NF-N-graphene hybrid leads to a significant enhancement in the catalytic performance of the pure Pt NFs. Therefore, the PNG-2-modified ITO electrode with a 0.05 mg ml^{-1} N-graphene loading exhibited the best catalytic performance with a detection limit of 0.34 μM between 1 μM and 1 mM. The EIS measurement confirmed that a further increase in the N-graphene loading up to 0.1 mg ml^{-1} led to an increase in the electrolyte-electrode interfacial resistance of the hybrid electrode, which results in a decrease in the electrocatalytic performance of the biosensor electrode due to an increase in agglomeration of N-graphene during the EPD.

Acknowledgements

This research is supported by the High Impact Research MoE Grant UM.C/625/1/HIR/MoE/SC/04 from the Ministry of Education Malaysia, UMRG Program RP012A-14SUS, RP038C-15HTM, Grand Challenge GC001C-14SBS and University Malaya Centre for Ionic Liquids (UMCiL). The work was also supported by Global Frontier R&D Program on Center for Wave Energy Control based on Metamaterials funded by the National Research Foundation under the Ministry of Science, ICT & Future Planning, Korea (No. 2014063711).

References

[1] S. Guo, D. Wen, Y. Zhai, S. Dong, E. Wang, Platinum nanoparticle ensemble-on- graphene hybrid nanosheet: one-pot, rapid synthesis, and used as new electrode material for electrochemical sensing, ACS Nano 4 (2010) 3959–3968.
[2] H. Wu, S. Fan, X. Jin, H. Zhang, H. Chen, Z. Dai, X. Zou, Construction of a zinc porphyrin–fullerene-derivative based nonenzymatic electrochemical sensor for sensitive sensing of hydrogen peroxide and nitrite, Anal. Chem. 86 (2014) 6285–6290.
[3] C. Kulp, K. Gillmeister, W. Widdra, M. Bron, Synthesis of CuCorePtShell nanoparticles as model structures for core–shell electrocatalysts by direct platinum electrodeposition on copper, ChemPhysChem 14 (2013) 1205–1210.
[4] B.P. Vinayan, R. Nagar, N. Rajalakshmi, S. Ramaprabhu, Novel Platinum–cobalt alloy nanoparticles dispersed on nitrogen-doped graphene as a cathode electrocatalyst for PEMFC applications, Adv. Funct. Mater. 22 (2012) 3519–3526.
[5] S. Liu, Z. Dai, H. Chen, H. Ju, Immobilization of hemoglobin on zirconium dioxide nanoparticles for preparation of a novel hydrogen peroxide biosensor, Biosens. Bioelectron. 19 (2004) 963–969.
[6] M. Mahmoudian, Y. Alias, W. Basirun, P.M. Woi, S. Baradaran, M. Sookhakian, Synthesis, characterization, and sensing applications of polypyrrole coated Fe 3 O 4 nanostrip bundles, Ceram. Int. 40 (2014) 9265–9272.
[7] A.T. Lawal, Synthesis and utilisation of graphene for fabrication of electrochemical sensors, Talanta 131 (2015) 424–443.
[8] M. Azarang, A. Shuhaimi, R. Yousefi, M. Sookhakian, Effects of graphene oxide concentration on optical properties of ZnO/RGO nanocomposites and their application to photocurrent generation, J. Appl. Phys. 116 (2014) 084307.
[9] S. Baradaran, E. Moghaddam, B. Nasiri-Tabrizi, W. Basirun, M. Mehrali, M. Sookhakian, M. Hamdi, Y. Alias, Characterization of nickel-doped biphasic calcium phosphate/graphene nanoplatelet composites for biomedical application, Mater. Sci. Eng. C-Mater. Biol. Appl. 49 (2015) 656–668.
[10] S. Gharehkhani, S.F.S. Shirazi, S.P. Jahromi, M. Sookhakian, S. Baradaran, H. Yarmand, A.A. Oshkour, S.N. Kazi, W.J. Basirun, Spongy nitrogen-doped activated carbonaceous hybrid derived from biomass material/graphene oxide for supercapacitor electrodes, RSC Adv. 5 (2015) 40505–40513.
[11] X. Li, X. Wang, L. Zhang, S. Lee, H. Dai, Chemically derived, ultrasmooth graphene nanoribbon semiconductors, Science 319 (2008) 1229–1232.
[12] Y. Xu, Z. Liu, X. Zhang, Y. Wang, J. Tian, Y. Huang, Y. Ma, X. Zhang, Y. Chen, A graphene hybrid material covalently functionalized with porphyrin: synthesis and optical limiting property, Adv. Mater. 21 (2009) 1275–1279.
[13] C.X. Guo, C.M. Li, A self-assembled hierarchical nanostructure comprising carbon spheres and graphene nanosheets for enhanced supercapacitor performance, Energy Environ. Sci. 4 (2011) 4504–4507.
[14] B. Seger, P.V. Kamat, Electrocatalytically active graphene-platinum nanocomposites. Role of 2-D carbon support in PEM fuel cells, J. Phys. Chem. C 113 (2009) 7990–7995.
[15] E. Yoo, J. Kim, E. Hosono, H.-s. Zhou, T. Kudo, I. Honma, Large reversible Li storage of graphene nanosheet families for use in rechargeable lithium ion batteries, Nano Lett. 8 (2008) 2277–2282.
[16] M. Sookhakian, Y.M. Amin, R. Zakaria, S. Baradaran, M.R. Mahmoudian, M. Rezayi, M.T. Tajabadi, W.J. Basirun, Enhanced photovoltaic performance of polymer hybrid nanostructure heterojunction solar cells based on poly (3-hexylthiophene)/ZnS/ZnO/reduced graphene oxide shell–core nanorod arrays, Ind. Eng. Chem. Res. 53 (2014) 14301–14309.
[17] M. Sookhakian, Y. Amin, R. Zakaria, W. Basirun, M. Mahmoudian, B. Nasiri-Tabrizi, S. Baradaran, M. Azarang, Significantly improved photocurrent response of ZnS-reduced graphene oxide composites, J. Alloy. Compd. 632 (2015) 201–207.
[18] M. Tajabadi, W. Basirun, F. Lorestani, R. Zakaria, S. Baradaran, Y. Amin, M. Mahmoudian, M. Rezayi, M. Sookhakian, Nitrogen-doped graphene-silver nanodendrites for the non-enzymatic detection of hydrogen peroxide, Electrochim. Acta 151 (2015) 126–133.
[19] Y. Wang, Y. Shao, D.W. Matson, J. Li, Y. Lin, Nitrogen-doped graphene and its application in electrochemical biosensing, ACS Nano 4 (2010) 1790–1798.
[20] Y. Shao, S. Zhang, M.H. Engelhard, G. Li, G. Shao, Y. Wang, J. Liu, I.A. Aksay, Y. Lin, Nitrogen-doped graphene and its electrochemical applications, J. Mater. Chem. 20 (2010) 7491–7496.
[21] X. Li, H. Wang, J.T. Robinson, H. Sanchez, G. Diankov, H. Dai, Simultaneous nitrogen doping and reduction of graphene oxide, J. Am. Chem. Soc. 131 (2009) 15939–15944.
[22] L. Panchakarla, K. Subrahmanyam, S. Saha, A. Govindaraj, H. Krishnamurthy, U. Waghmare, C. Rao, Synthesis, structure, and properties of boron-and nitrogen-doped graphene, Adv. Mater. 21 (2009) 4726–4730.
[23] M. Azarang, A. Shuhaimi, M. Sookhakian, Crystalline quality assessment, photocurrent response and optical properties of reduced graphene oxide uniformly decorated zinc oxide nanoparticles based on the graphene oxide concentration, RSC Adv. 5 (2015) 53117–53128.
[24] M.A.M. Teridi, M. Sookhakian, W.J. Basirun, R. Zakaria, F.K. Schneider, W.J. da Silva, J. Kim, S.J. Lee, H.P. Kim, A.R. bin Mohd Yusoff, Plasmon enhanced organic devices utilizing highly ordered nanoimprinted gold nanodisks and nitrogen doped graphene, Nanoscale 7 (2015) 7091–7100.
[25] G. Lu, G. Zangari, Electrodeposition of platinum on highly oriented pyrolytic graphite. Part I: electrochemical characterization, J. Phys. Chem. B 109 (2005) 7998–8007.
[26] A. Serov, N.I. Andersen, S.A. Kabir, A. Roy, T. Asset, M. Chatenet, F. Maillard, P. Atanassov, Palladium supported on 3D graphene as an active catalyst for alcohols electrooxidation, J. Electrochem. Soc. 162 (2015) F1305–F1309.
[27] Z. Zafar, Z.H. Ni, X. Wu, Z.X. Shi, H.Y. Nan, J. Bai, L.T. Sun, Evolution of Raman spectra in nitrogen doped graphene, Carbon 61 (2013) 57–62.
[28] J. Jin, X. Fu, Q. Liu, Y. Liu, Z. Wei, K. Niu, J. Zhang, Identifying the active site in nitrogen-doped graphene for the VO2+/VO2+ redox reaction, ACS Nano 7 (2013) 4764–4773.

[29] M. Mahmoudian, Y. Alias, W. Basirun, P.M. Woi, M. Sookhakian, Facile preparation of MnO 2 nanotubes/reduced graphene oxide nanocomposite for electrochemical sensing of hydrogen peroxide, Sens. Actuator B-Chem. 201 (2014) 526–534.
[30] M. Sookhakian, Y. Amin, S. Baradaran, M. Tajabadi, A.M. Golsheikh, W. Basirun, A layer-by-layer assembled graphene/zinc sulfide/polypyrrole thin-film electrode via electrophoretic deposition for solar cells, Thin Solid Films 552 (2014) 204–211.
[31] Y. Yang, R. Fu, J. Yuan, S. Wu, J. Zhang, H. Wang, Highly sensitive hydrogen peroxide sensor based on a glassy carbon electrode modified with platinum nanoparticles on carbon nanofiber heterostructures, Microchim. Acta 182 (2015) 2241–2249.
[32] L. Ding, B. Su, A non-enzymatic hydrogen peroxide sensor based on platinum nanoparticle–polyaniline nanocomposites hosted in mesoporous silica film, J. Electroanal. Chem. 736 (2015) 83–87.
[33] X. Bian, X. Lu, E. Jin, L. Kong, W. Zhang, C. Wang, Fabrication of Pt/polypyrrole hybrid hollow microspheres and their application in electrochemical biosensing towards hydrogen peroxide, Talanta 8 (2010) 813–818.
[34] S. He, Z. Chen, Y. Yu, L. Shi, A novel non-enzymatic hydrogen peroxide sensor based on poly-melamine film modified with platinum nanoparticles, RSC Adv. 4 (2014) 45185–45190.
[35] Y. Fang, D. Zhang, X. Qin, Z. Miao, S. Takahashi, J.I. Anzai, Q. Chen, A non-enzymatic hydrogen peroxide sensor based on poly (vinyl alcohol)—multiwalled carbon nanotubes—platinum nanoparticles hybrids modified glassy carbon electrode, Electrochim. Acta 70 (2012) 266–271.
[36] J. Wan, W. Wang, G. Yin, X. Ma, Nonenzymatic H_2O_2 sensor based on Pt nanoflower electrode, J. Cluster Sci. 23 (2012) 1061–1068.
[37] P. Wu, Z. Cai, Y. Gao, H. Zhang, C. Cai, Enhancing the electrochemical reduction of hydrogen peroxide based on nitrogen-doped graphene for measurement of its releasing process from living cells, Chem. Commun. 47 (2011) 11327–11329.